Molecular Microbiology (2012) 84(5), 816–831 ■
doi:10.1111/j.1365-2958.2012.08060.x
First published online 27 April 2012

A 95 kDa protein of *Plasmodium vivax* and *P. cynomolgi* visualized by three-dimensional tomography in the caveola–vesicle complexes (Schüffner's dots) of infected erythrocytes is a member of the PHIST family

Sheila Akinyi,[1†§] Eric Hanssen,[3,5§] Esmeralda V. S. Meyer,[1] Jianlin Jiang,[1] Cindy C. Korir,[1‡] Balwan Singh,[1] Stacey Lapp,[1] John W. Barnwell,[6] Leann Tilley,[4,5¶] Mary R. Galinski[1,2*¶]

[1]*Emory Vaccine Center, Yerkes National Primate Research Center, and* [2]*Department of Medicine, Division of Infectious Diseases, Emory University, Atlanta, GA, USA.*

[3]*Electron Microscopy Unit, Bio21 Molecular Science and Biotechnology Institute, and* [4]*Department of Biochemistry and Molecular Biology, Bio21 Molecular Science and Biotechnology Institute, The University of Melbourne, Melbourne, Vic. 3010, Australia.*

[5]*ARC Centre of Excellence for Coherent X-ray Science, The University of Melbourne, Melbourne, Vic. 3010, Australia.*

[6]*Malaria Branch, Division of Parasitic Diseases and Malaria, Centers for Disease Control and Prevention, Atlanta, GA, USA.*

Summary

***Plasmodium vivax* and *P. cynomolgi* produce numerous caveola–vesicle complex (CVC) structures within the surface of the infected erythrocyte membrane. These contrast with the electron-dense knob protrusions expressed at the surface of *Plasmodium falciparum*-infected erythrocytes. Here we investigate the three-dimensional (3-D) structure of the CVCs and the identity of a predominantly expressed 95 kDa CVC protein. Liquid chromatography – tandem mass spectrometry analysis of immunoprecipitates by monoclonal antibodies from *P. cynomolgi* extracts identified this protein as a member of the *Plasmodium* helical interspersed subtelomeric (PHIST) superfamily with a calculated mass of 81 kDa. We named the orthologous proteins PvPHIST/CVC-81$_{95}$ and PcyPHIST/CVC-81$_{95}$, analysed their structural features, including a PEXEL motif, repeated sequences and a C-terminal PHIST domain, and show that PHIST/CVC-81$_{95}$ is most highly expressed in trophozoites. We generated images of CVCs in 3-D using electron tomography (ET), and used immuno-ET to show PHIST/CVC-81$_{95}$ localizes to the cytoplasmic side of the CVC tubular extensions. Targeted gene disruptions were attempted *in vivo*. The *pcyphist/cvc-81$_{95}$* gene was not disrupted, but parasites containing episomes with the *tgdhfr* selection cassette were retrieved by selection with pyrimethamine. This suggests that PHIST/CVC-81$_{95}$ is essential for survival of these malaria parasites.**

Accepted 28 March, 2012. *For correspondence. E-mail mary.galinski@emory.edu; Tel. (+1) 404 727 7214; Fax (+1) 404 727 8199. Present addresses: †Department of Parasitic Diseases and Malaria, Centers for Disease Control and Malaria, Atlanta, GA 30083, USA; ‡Kimberly-Clark Corporate Research and Engineering, Roswell, GA 30076, USA. §These individuals contributed equally to this research as first authors. ¶These individuals contributed equally to the development of this research as senior authors.

Introduction

Malaria, an infectious disease caused predominantly by *Plasmodium vivax* and *P. falciparum*, results in illness in more than 200 000 000 people each year in 106 countries (WHO, 2011). The parasite undergoes a cyclical process of invading, thriving within and rupturing host erythrocytes. During the blood-stage of the disease, the merozoite form of the parasite efficiently enters host red blood cells (RBCs), grows and multiplies to create new asexual progeny, and also differentiates to generate sexual-stage parasites. Pathogenic processes ensue in the host, with resulting organ damage, anaemia and associated medical complications (reviewed in Mueller *et al.*, 2009; Price *et al.*, 2009; Rowe *et al.*, 2009). The biological mechanisms used by *P. vivax* and *P. falciparum* to invade, grow and survive inside RBCs have important species-specific differences, which are largely unexplored. Research on *P. vivax* has trailed far behind *P. falciparum*, and comparative studies have been few.

As a merozoite is invading a target host RBC it creates a parasitophorous vacuole (PV) (reviewed in Galinski *et al.*, 2005). The parasite grows within the PV, surrounded by a

PV membrane, the host RBC cytoplasm and host RBC membrane. Although the uninfected, enucleated RBC lacks protein synthesis and trafficking machinery, the parasite has the capacity to produce and transport proteins to the PV membrane and onwards using specialized structures it develops in the RBC cytoplasm and at the surface of the infected RBC (iRBC) membrane. Investigations in this area of malaria biology are most advanced for *P. falciparum*, resulting in many breakthroughs in the scientific understanding of transport biology in this species (reviewed in Tilley *et al*., 2008; 2011; Maier *et al*., 2009; Haase and de Koning-Ward, 2010). Research on *P. falciparum* blood-stage biology has been aided since 1976 by the availability of robust *in vitro* culture systems (Trager and Jensen, 1976), and, over the last decade by a *P. falciparum* genome database (Gardner *et al*., 2002) and a variety of functional genome technologies (reviewed in Di Girolamo *et al*., 2005; Aurrecoechea *et al*., 2009). A growing body of knowledge now exists relating to the structure and composition of *P. falciparum*-induced cytoplasmic membranous structures that develop between the PV and the surface of the iRBC. Notably, the *P. falciparum* iRBC membrane surface also becomes studded with electron-dense structures known as knobs, which contain erythrocyte membrane protein-1 (PfEMP-1), the antigenically variant virulence protein that is encoded by the large *var* multigene family (reviewed in Scherf *et al*., 2008). Recently, electron tomography (ET) has been employed for imaging *P. falciparum* iRBCs, and this technology has enabled three-dimensional (3-D) imaging of the whole iRBC, Maurer's cleft organelles and the discovery of tethers bridging them to the iRBC membrane (Hanssen *et al*., 2008; 2011).

In contrast to developing protruding knob structures, peppered along the surface of the iRBC host membrane, *P. vivax* induces a pitted membrane surface with the formation of numerous flask-shaped indentations of the iRBC membrane, called caveolae, in association with vesicles. These unique intricate structures, termed caveola–vesicle complexes (CVCs), were first observed by transmission electron microscopy (TEM) in 1975 (Aikawa *et al*., 1975) and described as 90–100 nm wide caveolae with several 40–50 nm wide electron-dense vesicles extending from the caveolar base. Some vesicles appear alveolar in shape, while others are elongated and tubular (Aikawa *et al*., 1975). These studies, which focused on the iRBC membranes of *P. vivax* and the simian malaria parasite *Plasmodium cynomolgi*, a species that is genetically very close to *P. vivax* (Waters *et al*., 1993), also established that the caveolae structures are open to the exterior of the host cell and physically accumulate Giemsa stain resulting in the abundant reddish speckled appearance in *P. vivax* iRBCs treated with Romanowsky-based stains known as Schüffner's stippling (Schüffner, 1899). CVCs have since also been confirmed by TEM to be present in the human malaria species *Plasmodium ovale* (Aikawa *et al*., 1977; Matsumoto *et al*., 1986), and, based on similar Giemsa-stained patterns, they are presumed to be present in at least three other non-human primate species of *Plasmodium* (*P. fieldi*, *P. simiovale* and *P. gonderi*); the iRBCs of each of these species are similarly characterized by profuse Schüffner's like stippling of Giemsa-stained iRBCs in blood smears (Coatney, 1971).

How CVC form and the functional purpose of these abundant membrane structures are not known, although it has been suggested that they may function in nutrient transport or release of parasite metabolites from infected erythrocytes (Aikawa *et al*., 1975; Matsumoto *et al*., 1988; Udagama *et al*., 1988). Limited exploratory biochemical studies confirmed that they can provide a means for metabolic exchange of the parasitized cell with the host plasma (Aikawa *et al*., 1975). Lactoperoxidase catalysed ^{125}I surface examination, metabolic radiolabelling experiments and immunobiochemical studies verified that the CVCs are in part comprised of a 95 kDa and other specific parasite-derived proteins (Barnwell, 1986; Udagama *et al*., 1988; Barnwell *et al*., 1990). However, the composition, developmental origin, and function(s) of the CVCs remain otherwise largely unexplored. The simian malaria species *Plasmodium knowlesi*, which is also related to *P. vivax*, in contrast, only produces a few caveolae at the surface of the iRBCs, without associated alveolar or tubular vesicles (Aikawa *et al*., 1975).

Investigations relating to the unique species-specific modifications of *P. vivax* iRBCs and corresponding transport biology have not progressed in parallel with similar lines of research on *P. falciparum* iRBCs. This is largely because continuous *in vitro* blood-stage culture systems and routine functional genetic technologies have not been established for studies of *P. vivax* or for *P. cynomolgi*, which serves as an effective and reliable experimental model for *P. vivax* (reviewed in Galinski and Barnwell, 2008; 2012). Moreover, the first *P. vivax* genome sequence and associated database was published only recently (Carlton *et al*., 2008), and a *P. cynomolgi* genome sequence has not yet been published. While functional genomics for these species is in its experimental infancy, initial successful transient transfections of *P. vivax* (Pfahler *et al*., 2006) and *P. cynomolgi* (Kocken *et al*., 1999) iRBCs have been reported in experimental infections of non-human primates.

In the present study, we aimed to investigate the 95 kDa protein that was shown to be a predominant parasite-derived component exclusively associated with the CVCs in *P. vivax* iRBCs (Barnwell *et al*., 1990), and also examine the structure of the CVCs for the first time in 3-D. Liquid chromatography – tandem mass spectrometry (LC-MS/MS) analysis of this protein immunoprecipitated from

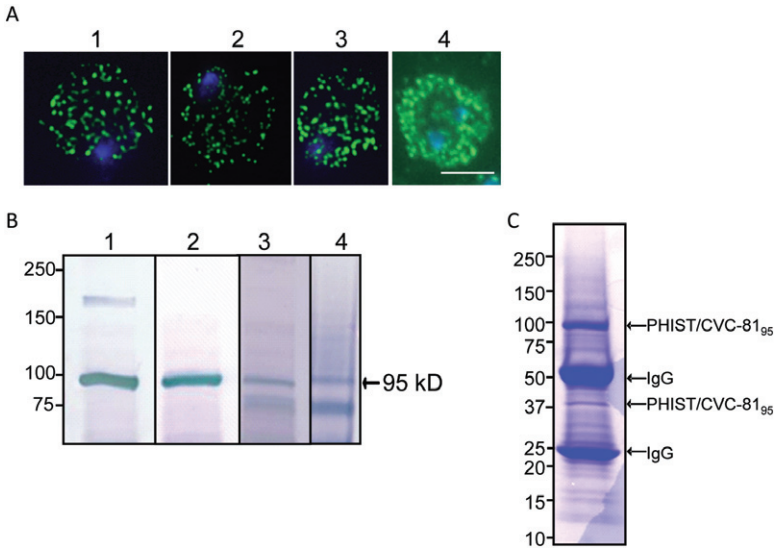

Fig. 1. The predominant 95 kDa CVC protein is a member of the PHIST protein superfamily.
A. Air-dried, acetone-fixed smears of *P. cynomolgi* trophozoite iRBCs incubated with the nuclear DAPI stain (blue) and *P. vivax* mAbs 4C12.G4 (1), 2H8.E10 (2), 2H12.B4 (3) and 1H4.B6 (4) followed by Alexa Fluor 488-conjugated goat anti-mouse IgG (Invitrogen) (green). Immunofluorescence was detected using a Zeiss Imager.Z1 microscope (panels 1–3), and Zeiss Axioskop 2 (panel 4). Scale bar: 4 μm.
B. *P. cynomolgi* trophozoite iRBC extracts were separated by SDS-PAGE under reducing conditions on a 4–20% gradient gel, transferred to a nitrocellulose membrane, and probed with *P. vivax* mAbs 2H12.B4, 4C12.G4, 2H8.E10 and 1H4.B6. A characteristic band of 95 kDa (Barnwell *et al*., 1990) was consistently obtained with all four mAbs (lanes 1–4), and a predominant breakdown product at 75 kDa with some extracts (lanes 3 and 4). Lanes 1 and 2, and 3 and 4 represent different extracts.
C. LC-MS/MS was performed on bands excised from 4–20% SDS-PAGE gels containing proteins from *P. cynomolgi* trophozoite iRBC extracts immunoprecipitated with mAbs 2H12.B4, 4C12.G4, 2H8.E10 and 1H4.B6; a representative experiment using mAb 1H4.B6 is shown. The proteins identified by LC-MS/MS are noted as PHIST/CVC-81$_{95}$ or IgG.

detergent extracts of *P. cynomolgi* iRBC using monoclonal antibodies (mAbs) revealed it to be a member of the *Plasmodium* helical interspersed subtelomeric (PHIST) superfamily of proteins (Sargeant *et al*., 2006) with a calculated mass of 81 kDa. Electron tomograms are presented showing the elaborate multi-vesicular/tubular nature of the parasite's CVCs and confirming the presence of the 95 kDa protein, now termed PHIST/CVC-81$_{95}$, specifically on the cytoplasmic side of the tubules. Finally, we demonstrate that the PHIST/CVC-81$_{95}$ protein appears to be required for growth of the parasite. Transfected *P. cynomolgi* parasites could be retrieved from *in vivo* rhesus monkey blood-stage infections after applying pyrimethamine drug pressure, with episomes containing the *pcyphist/cvc-81$_{95}$* knockout (KO) construct and the *tgdhfr* drug selection cassette, but we were not able to achieve disruption of the *pcyphist/cvc-81$_{95}$* gene.

Results

Proteomic identification of the predominant P. vivax *95 kDa CVC protein as a member of the PHIST superfamily by detection and analysis of its homologue in* P. cynomolgi *iRBCs*

A subset of mAbs developed against mature *P. vivax* iRBCs were shown previously to target specifically the CVCs in *P. vivax* iRBC membranes and to immunoprecipitate from SDS extracts of iRBCs a predominant *P. vivax* antigen that migrated at 95 kDa in SDS-PAGE (Barnwell, 1986; Barnwell *et al*., 1990). Several of these mAbs were also reported at the time to cross-react in indirect immunofluorescence assays (IFAs) with *P. cynomolgi* iRBCs. *P. cynomolgi* iRBCs are easily generated in large quantities from rhesus monkey infections and therefore more amenable to in-depth study than *P. vivax* attained from small New World monkey infections or clinical isolates. We set out in the current studies to use four of the mAb reagents in proteomic experiments to identify the associated gene in *P. cynomolgi* and further investigate the structure, location and function of this predominant protein in the context of the CVCs. To proceed, first we reconfirmed the cross-reactivity of mAbs 2H12.B4, 2H8.E10, 4C12.G4 and 1H4.B6 with *P. cynomolgi* trophozoite iRBCs (Fig. 1A). The typical fluorescence pattern representative of CVCs with a dense pattern of speckling was reliably produced. These heavily dotted patterns mimic the classic spread of pink to dark red dots of Schüffner's stippling observed throughout *P. vivax* and *P. cynomolgi* iRBCs in Giemsa-stained thin blood smears.

We confirmed that all four mAbs (2H12.B4, 2H8.E10, 4C12.G4 and 1H4.B6) recognized the expected 95 kDa antigen, in SDS extracts of *P. cynomolgi* iRBCs by

immunoblot analysis (Fig. 1B), and immunoprecipitated the corresponding protein and associated breakdown products. The *P. cynomolgi* 95 kDa protein was immunoprecipitated with each mAb, excised and processed from the SDS-PAGE gel slices and analysed by LC-MS/MS. The resulting peptide sequences were searched against the *P. vivax* genome database and the gene ID: PVX_093680 (annotated as a member of the PHIST superfamily; Sargeant *et al*., 2006) was identified with each antibody reagent. This PHIST protein, like all known members of the superfamily, is characterized by the presence of a PHIST domain, containing multiple predicted alpha-helical domains and several conserved tryptophan residues. A representative immunoprecipitation result using mAb 1H4.B6 is shown in Fig. 1C, with the detection of the 95 kDa PHIST protein and a breakdown product at 37 kDa; the other major protein bands were verified by LC-MS/MS to be IgG. The MASCOT tool was used to search the *P. vivax* proteome database and the gene ID: PVX_093680 was identified with at least 22 spectral counts, 10 unique and no shared peptides. PVX_093680 has 2133 nucleotides (nt) of coding sequence and is contained within two exons. The 710-amino-acid protein has a calculated mass of 80.73 kDa, lower than the 95 kDa extrapolated from its relative electrophoretic mobility in SDS-PAGE gels. Such differences are not unusual for *Plasmodium* antigens, which depending on the amino acid composition and imposed secondary structure can (and more often than not) migrate quite different from their calculated molecular masses.

To maintain the original designation of this protein as a 95 kDa antigen determined by SDS-PAGE (Barnwell *et al*., 1990), and recognize the calculated molecular mass of 81 kDa, we hereafter refer to this protein in *P. vivax* and *P. cynomolgi* respectively as PvPHIST/CVC-81_{95} and PcyPHIST/CVC-81_{95}.

PvPHIST/CVC-81_{95} and PcyPHIST/CVC-81_{95} lack species-specific repeated motifs present in other species while conservation of the PHIST domain is retained across species

Fifty-two amino acids downstream of the N-terminus, PvPHIST/CVC-81_{95} has a 22-amino-acid hydrophobic region. According to bioinformatic analyses using the MalSig algorithm (http://www.masig.biochem.unimelb.edu.au/), this region may serve as a recessed signal sequence or signal anchor. A predicted *Plasmodium* export element (PEXEL; RxLxE/Q/D; Hiller *et al*., 2004; Marti *et al*., 2004) follows approximately 12 amino acids downstream of this hydrophobic domain; this sequence has been shown to be important for the trafficking of some but not necessarily all proteins from the PV onwards to the surface of the iRBC (Spielmann and Gilberger, 2010). The protein's PHIST domain is at the C-terminal portion of the protein, with four predicted alpha-helical domains and four positionally conserved tryptophan residues (Sargeant *et al*., 2006). PvPHIST/CVC-81_{95} can also be classified as aspartate (11.7%) and glycine (11%) rich (http://ca.expasy.org/tools/protparam.html) due to the presence of remnants of degenerated repeated nucleotide sequence motifs within the central region of the gene (discussed further below) that encode a comparatively high number of these amino acids. Arginine and proline residues are also relatively high at 11.4% and 11% respectively.

To support continued in-depth investigations of PvPHIST/CVC-81_{95} and the biological and functional analysis of CVCs, we proceeded to identify and characterize the orthologous gene in the experimental model *P. cynomolgi*. The absence of a *P. cynomolgi* genome database at the time of this work necessitated a traditional scheme to identify and characterize the *pcyphist/cvc-81_{95}* gene using polymerase chain reaction (PCR) and standard DNA sequencing methods. First, *pvphist/cvc-81_{95}* homologues were detected in *P. falciparum* and the simian malaria species *P. knowlesi* through BLAST (Basic Linear Alignment Search Tool) nucleotide searches of the PlasmoDB database (http://plasmodb.org). The most closely related sequences identified have the respective gene IDs: Pf08_0137 [annotated as *Plasmodium* exported protein (PHISTc)] and PkH_011720, with calculated molecular masses of 147 kDa and 105 kDa respectively; thus referred to here with the comparable PfPHIST-147 and PkPHIST-105 nomenclature. Both were annotated in the PlasmoDB database as proteins of unknown function. BLAST analyses of the NCBI database (http://www.ncbi.nlm.nih.gov/protein/) were also performed using the PvPHIST/CVC-81_{95} amino acid sequence to reveal distant homologues from rodent malaria parasite species. *Plasmodium yoelii* (gene ID: Py01786) and *P. berghei* [duplicated gene IDs: PB108348.00.0 and PB000848.03.0 (Sargeant *et al*., 2006)] homologues were identified; unlike the primate malaria parasite species, a family of paralogous genes is not present in these rodent parasite species.

Degenerate gene-specific and 3′ UTR primer pairs were subsequently designed based on *pvphist/cvc-81_{95}* coding and non-coding regions (see *Experimental procedures*) and the most closely related corresponding gene sequence from *P. knowlesi* (PkH_011720; *pkphist-105*). Subsequently, PCR amplification and cDNA sequencing experiments were performed to successfully identify the orthologue from *P. cynomolgi*. Our analyses verified the *pcyphist/cvc-81_{95}* gene to be 2433 nt, encoding a 720-amino-acid protein on two exons, with a similar basic structure as exists for the *P. vivax*, *P. falciparum* and *P. knowlesi* homologues (Fig. 2A). Notably, each has a hydrophobic sequence at the end of the first exon, a putative PEXEL motif (Marti *et al*., 2004) at the beginning

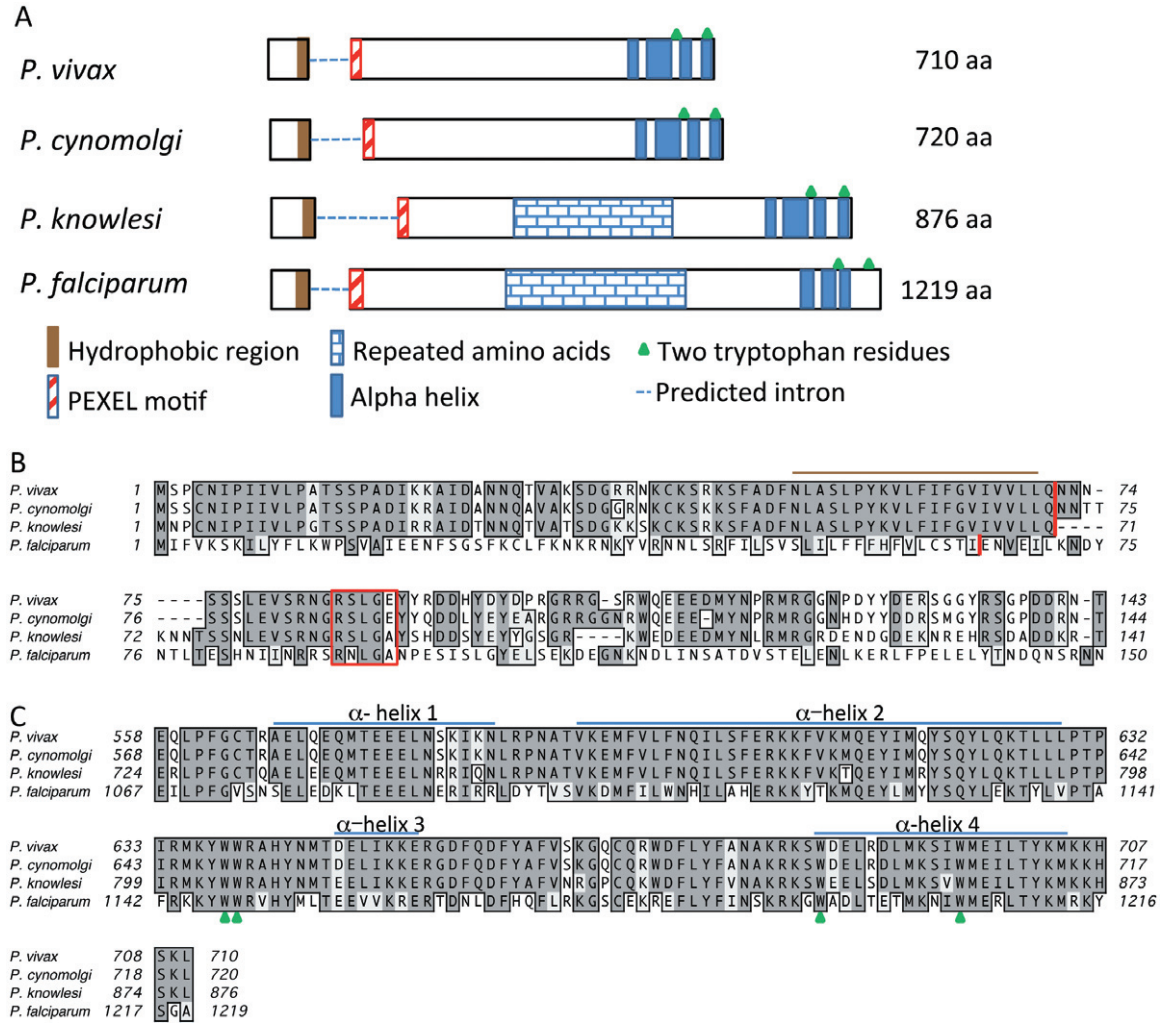

Fig. 2. Protein structure and sequence identity of PcyPHIST/CVC-81$_{95}$ and its homologues.
A. The schematic represents the PvPHIST/CVC-81$_{95}$, PcyPHIST/CVC-81$_{95}$, PkPHIST-105 and PfPHIST-147 proteins, showing their number of amino acids and main features as indicated.
B and C. N- and C-terminal amino acid sequence alignments generated using CLUSTALW. Positions of identity across all four species are shown in dark grey; the hydrophobic sequence is marked by a brown line; the putative PEXEL motif is boxed in red; and the conserved tryptophans are denoted with a green triangle. The four regions predicted using the GOR4 algorithm (Combet *et al.*, 2000) to form alpha-helices are shown within the blue boxes.

of exon II, a central region predominated by a variety of degenerated repeated sequences, and a conserved C-terminal PHIST domain with four characteristic alpha-helical domains and four tryptophan residues (Fig. 2A).

Our analysis shows that each of these proteins can be classified as members of the PHISTc subfamily, based on the positioning of the four conserved tryptophans within the PHIST domain (Sargeant *et al.*, 2006). In the *P. cynomolgi* gene, a 270 nt intron separates the short initial exon of 213 nt from the second exon of 1950 nt. The size of the exons and introns differs for each species, yet conserved sequence motifs and features define the homologues (Fig. 2B; the *P. knowlesi phist-81$_{95}$* intron-exon boundaries are based on RNA sequencing information; J. Rayner and M. Galinski, unpubl. data). Table 1 shows the percentage of identities found at the nucleotide and amino acid levels when the entire *P. vivax* and *P. cynomolgi*

Table 1. Identity between PvPHIST/CVC-81$_{95}$ and PcyPHIST/CVC-81$_{95}$.

	Nucleotide	Amino acid
Global	83%	75%
5′/N-terminal	92%	93%
Central	74%	56%
3′/C-terminal	100%	100%

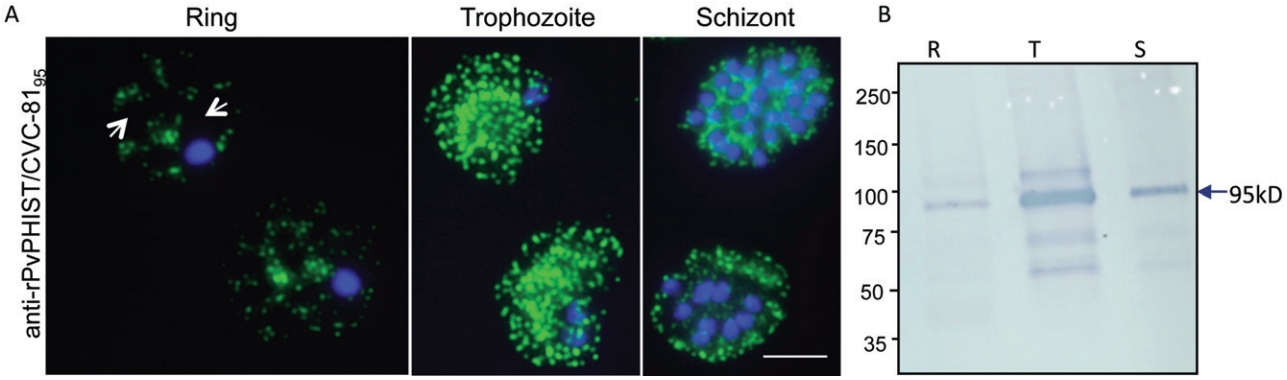

Fig. 3. PcyPHIST/CVC-81$_{95}$ is expressed in the ring, trophozoite and schizont stages of development.
A. IFA tests. Air-dried and acetone-fixed smears of ring-, trophozoite- and schizont-stage *P. cynomolgi* iRBCs were incubated with rabbit anti-rPvPHIST/CVC-81$_{95}$ serum and mounted in Prolong Gold Antifade Reagent containing the nuclear DAPI stain (Invitrogen; blue). Positive antibody reactivity was detected using Alexa Fluor 488-conjugated anti-rabbit IgG (Invitrogen, green). The ring-stage panel illustrates a 'soccer ball' pattern of PHIST reactivity; white arrows point to blackened areas lacking fluorescence. Immunofluorescence was detected using a Zeiss Imager.Z1 microscope. Scale bar: 0.4 μm.
B. Western immunoblot. SDS detergent extracts from 1×10^8 *P. cynomolgi* ring-, trophozoite- and schizont-stage iRBC pellets were diluted 1:100 in sample buffer and subjected to SDS-PAGE under non-reducing conditions on a 4–20% gradient gel. Rabbit anti-rPvPHIST/CVC-81$_{95}$ was used at a 1:1000 dilution.

PHIST/CVC-81$_{95}$ sequences were aligned, compared with the three separate regions comprising these molecules at the DNA (5′ coding, central and 3′ coding regions) and protein (N-terminal, central and C-terminal regions) levels. The N-terminal 155-amino-acid regions (92%), and especially the C-terminal 155-amino-acid regions (100%) encoding the PHIST domain, are highly conserved compared with the central region of the protein. CLUSTAL alignments highlighting the relationship of the N-terminal and C-terminal regions of PvPHIST/CVC-81$_{95}$, PcyPHIST/CVC-81$_{95}$, PkPHIST-105 and PfPHIST-147 proteins are shown in Fig. 2B and C. Supporting information includes the sequences and alignments of these proteins, including the *P. berghei* and *P. yoelii* rodent parasite orthologues (Figs S1 and S2). When the C-terminal PHIST domains are compared across all species at least three of four alpha-helical domains (helix-1, -2 and -3) align, and the tryptophan residues are conserved in number in all species, including the rodent parasites (Fig. S1). The degenerate repeated motifs are readily apparent in the PfPHIST-147 and PkPHIST-105 proteins, and the rodent parasite PHIST proteins, but not in PvPHIST/CVC-81$_{95}$ and PcyPHIST/CVC-81$_{95}$. Only a few small four-amino acid motifs (HDGX) are present in the *P. vivax* sequence and as well a number of doublets (e.g. DD, PP and GG) are repeated a few times in the central regions of both PvPHIST/CVC-81$_{95}$ and PcyPHIST/CVC-81$_{95}$. This suggests that the central regions of these genes are undergoing evolutionary changes that are not constrained by the requirement for strict conservation of the central domain. To the contrary, we hypothesize that the central regions of the PvPHIST/CVC-81$_{95}$ and PcyPHIST/CVC-81$_{95}$ proteins may have evolved to accommodate specific roles of these proteins in *P. vivax* and *P. cynomolgi* CVCs.

PcyPHIST/CVC-81$_{95}$ is expressed throughout the erythrocytic stages in P. cynomolgi*, predominantly in trophozoites*

Once the *pvphist/cvc-81$_{95}$* and *pcyphist/cvc-81$_{95}$* genes and predicted proteins were identified and analysed, a recombinant protein representing all 710 amino acids encoded by *pvphist/cvc-81$_{95}$* (rPvPHIST/CVC-81$_{95}$) was expressed in *Escherichia coli* and used to produce a polyclonal rabbit antiserum (anti-rPvPHIST/CVC-81$_{95}$). This antiserum was evaluated in immunofluorescence microscopy on thin blood smears containing *P. cynomolgi* iRBCS in different stages of its ~ 48 h cycle. An immunofluorescence pattern of small dots spotted across the iRBC was evident beginning with moderate density at the ring stage of development. The speckling became greatly increased in abundance and intensity in the trophozoite and schizont stages (Fig. 3A). Rabbit pre-immune serum was negative for all stages (data not shown). PcyPHIST/CVC-81$_{95}$ was also detected by western immunoblot assays in each of these developmental stages with maximal expression apparent at the mature trophozoite stage (Fig. 3B). Interestingly, at the ring stage of development when the fluorescent labelled dots are sparser in number, an imperfect hexagonal plate or so-called 'soccer ball' pattern of fluorescence was frequently apparent, with fluorescent areas intermixed with dark areas lacking fluorescence (Fig. 3A, panel 1, arrows).

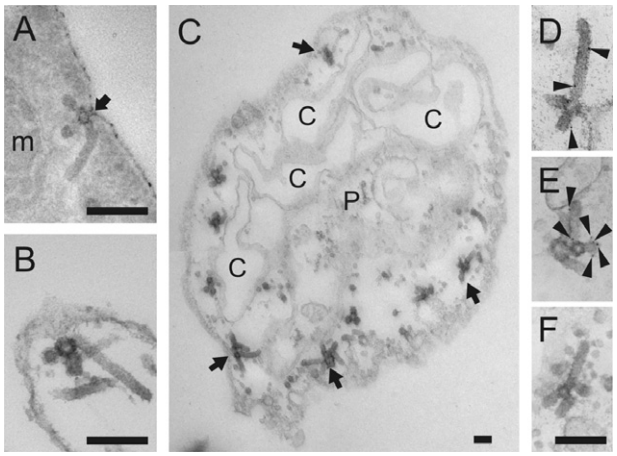

Fig. 4. Transmission electron microscopy of intact and permeabilized *P. cynomolgi* iRBCs.
A. An intact iRBC showing one CVC at the surface (arrow); note the presence of a mitochondrion (m).
B. An EqtII permeabilized iRBC section showing one CVC with several long extensions.
C. Low-magnification image showing a section of a whole EqtII-permeabilized iRBC showing the presence of multiple CVCs (several indicated with arrows), clefts (C) and parasite (P).
D–F. Immunolabelling (denoted with arrowheads) of CVCs in EqtII permeabilized iRBCs using mAb 4C12.G4 (D), rabbit anti-rPvPHIST/CVC-8195 (E) and a negative control (F).
Scale bars: 200 nm.

Immuno-ET reveals elaborate 3-D signatures of the CVCs from P. cynomolgi *iRBCs and localizes PcyPHIST/CVC-81$_{95}$ to the cytoplasmic side of the tubular extensions*

Transmission electron microscopy of CVCs in cross-sectional analysis of *P. vivax* and *P. cynomolgi* iRBCs provide an incomplete picture of the physical nature of these organelles (Aikawa *et al*., 1975; Matsumoto *et al*., 1988; Udagama *et al*., 1988; Barnwell *et al*., 1990). Particularly with the definition of specific CVC proteins and antisera in hand, we became interested in exploring the CVC structures visually in 3-D space and determining the localization of the predominant *PcyPHIST/CVC-81$_{95}$* protein using immuno-ET methods. ET enables the generation of 3-D images and we have previously shown this to be a powerful technique for visualizing internal membranous structure and organelles in *P. falciparum* iRBCs (Hanssen *et al*., 2008; 2010). Thus, *P. cynomolgi* trophozoite iRBC samples were processed in a similar manner, using equinatoxin II (EqtII) (Anderluh *et al*., 1996; Jackson *et al*., 2007) treatment to release haemoglobin and allow entry of antibodies. Transmission electron micrographs and 3-D electron tomograms from intact and EqtII-permeabilized cells were generated (Figs 4 and 5). The images revealed an elaborate structural nature of the CVCs. A caveolar 'cup' with an electron-dense coat remains open to the surface of the iRBC and provides an open connection to a variable number of coated vesicles and tubules. The average width of the tubular structures is 40 nm, while the vesicles range in average diameter from 25 to 45 nm. Additional vesicles with similar diameters appear to be located close to the CVCs. The structures are similar in intact and EqtII-permeabilized iRBCs indicating that this procedure does not compromise the CVC membrane structure, while permitting improved contrast. Other membranous structures are observed including Maurer's cleft-like structures (Fig. 4C) and host cell mitochondria (Fig. 4A) consistent with the preference of *P. cynomolgi*, like *P. vivax*, for invading reticulocytes (reviewed in Galinski and Barnwell, 2008; 2012).

We demonstrate that PcyPHIST-81$_{95}$ is associated with the CVCs of *P. cynomolgi* trophozoite iRBCs. Equinatoxin II-permeabilized iRBCs were labelled with mAb 4C12.G4 (Figs 4D and 6A–D) and anti-rPvPHIST/CVC-81$_{95}$ serum (Figs 4E and 6E–H). The 4C12.G4 gold-labelled mAb localized to CVCs, as previously observed by immuno-TEM experiments with *P. vivax* iRBCs (Barnwell *et al*., 1990). The labelling indicates that the epitope is present on the cytoplasmic side of the tubular extensions of the CVCs (Fig. 6D and H).

We have used IMOD to stitch serial 3-D reconstructed tomograms of a region of a *P. cynomolgi* iRBC containing CVCs. The interconnected nature of the caveolar opening of the CVC, the body of the caveola and the connected multiple tubular extensions can be appreciated by examining individual sections from the electron tomograms (Figs 5 and 6) or by translating through the sections (Videos S1 and S3). Each CVC has a unique 'morphological signature', differing in the number and sizes of vesicles and tubules. IMOD was used to render the surface of the CVCs and 3-D rotations are presented in Videos S2 and S4. The caveolar opening is rendered in blue and the tubule-vesicular extensions in orange.

Genetic manipulation of P. cynomolgi *with a* pcyΔphist/cvc-81$_{95}$ *vector*

Given the predominance of the PvPHIST/CVC-81$_{95}$ and PcyPHIST/CVC-81$_{95}$ proteins in the iRBC membrane and as a component of the CVCs (Barnwell *et al*., 1990), we hypothesized that this protein would prove to be essential for the parasite's survival. To test this hypothesis, we carried out two transfection experiments aiming to target and knock out the *pcyphist/cvc-81$_{95}$* gene. The *pcyΔphist/cvc-81$_{95}$* KO cassette was designed to target 600 bp at the 5′ end and 554 bp at the 3′ end of the *pcyphist-81$_{95}$* gene (Fig. 7A). This construct also contains the mutated *tgdhfr-ts* gene flanked by the *P. berghei dhfr* 5′ promoter and 3′ UTR regions to drive expression of the DHFR protein and confer pyrimethamine resistance. The *pcyΔphist/cvc-81$_{95}$* vector was digested with BamHI and

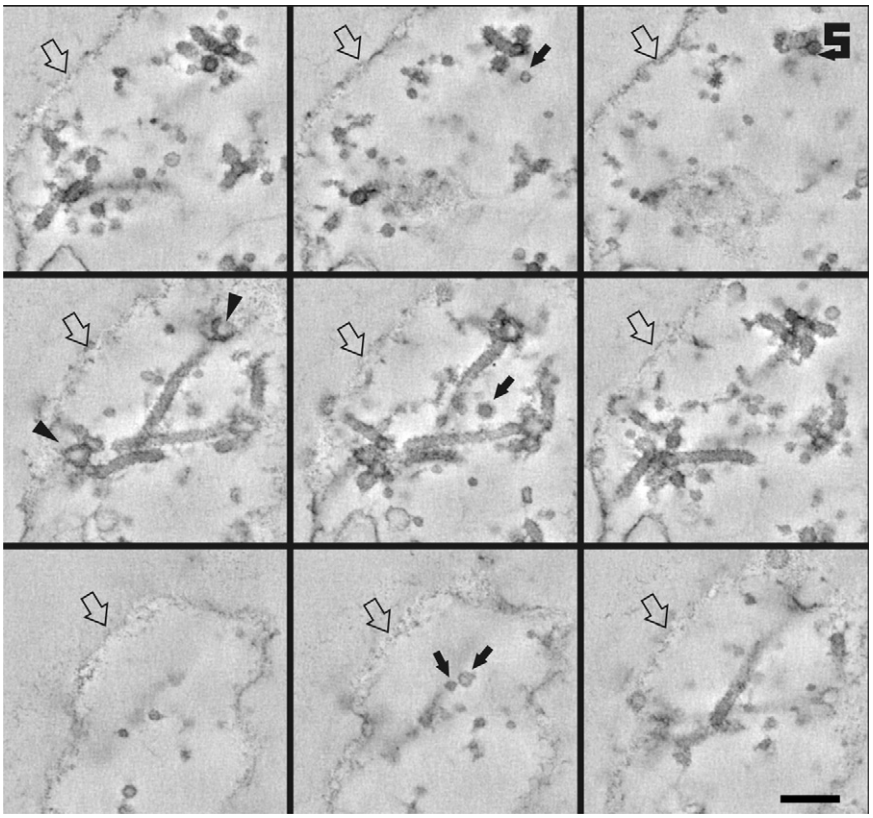

Fig 5. Electron tomography of CVCs in a *P. cynomolgi* trophozoite iRBC. Virtual sections through an approximately 200-nm-thick tomogram are presented. Each image represents a thickness of 2.7 nm and the spacing between each image is 18 nm. *P. cynomolgi* trophozoite iRBCs were permeabilized with EqtII and prepared for electron tomography. A dual tilt series was collected every 1.5° for the first axis and every 3° for the second axis, and used to generate a 3-D volume. Caveolar openings are indicated with arrowheads. The RBC membrane is indicated with an open arrow, and isolated vesicles with diameters ranging from 25 to 45 nm are noted with black arrows. The sequence of images is from the top right to bottom left, as indicated by a directional arrow in the top right panel. Scale bar: 200 nm.

EcoRI to release the KO cassette from its pUC19 backbone vector. The released, linearized constructs were visualized by agarose gel electrophoresis (Fig. 7B). Each electroporation was performed using a suspension of *P. cynomolgi* schizont iRBCs enriched from blood collected from an infected donor rhesus monkey. Transfected iRBCs were immediately reconstituted in incomplete RPMI-1640 and inoculated into a recipient rhesus monkey.

Parasitaemia in recipient monkeys from two sequential experiments were monitored daily by microscopic analysis of thick and thin blood smears. For the first experiment, the parasitaemia increased to 0.63% on day 3 and the first dose of pyrimethamine was administered. The drug was administered again on days 4 and 10. Parasites were not subsequently observed until day 14. Additional pyrimethamine doses were administered on days 17 and 18, to continue to select for parasites harbouring the mutated *tgdhfr-ts* gene. The parasitaemia increased to 3.1% by day 24, and the infected blood was collected, and stored. For the second experiment the parasitaemia increased to 1.2% on day 6 and the first dose of pyrimethamine was administered. The drug was administered again on days 7, 8, 13, 14, 19, 20, 24 and 25. Selected parasites were observed by day 18. The parasitaemia increased to 2.6% by day 25, and the infected blood was collected, and stored on day 26. Graphs of these parasitaemias are shown in Fig. S3.

Genomic DNA (gDNA) of the recovered parasites was extracted and used as a template for PCR amplification to assess the integration status of the *pcyΔphist/cvc-81*$_{95}$ cassette, using *pcyphist/cvc-81*$_{95}$ forward and reverse primers (Fig. 7B). Despite the retrieval of pyrimethamine-resistant parasites, these PCR tests were negative, indicating the lack of genomic integration of the *pcyΔphist/cvc-81*$_{95}$ cassette. Southern blots experiments were also consistent with the lack of integration (not shown). We then questioned whether episomes, possibly resulting from a low copy number of undigested plasmids in the electroporation mixture, were conferring resistance to the drug. To address this question, DNA from the transfected parasites was extracted using a QIAgen miniprep kit for plasmid purification. Plasmid DNA was retrieved from the iRBCs and used to transform TOP10 *E. coli* cells (Invitrogen). Plasmid DNA was purified and digested with

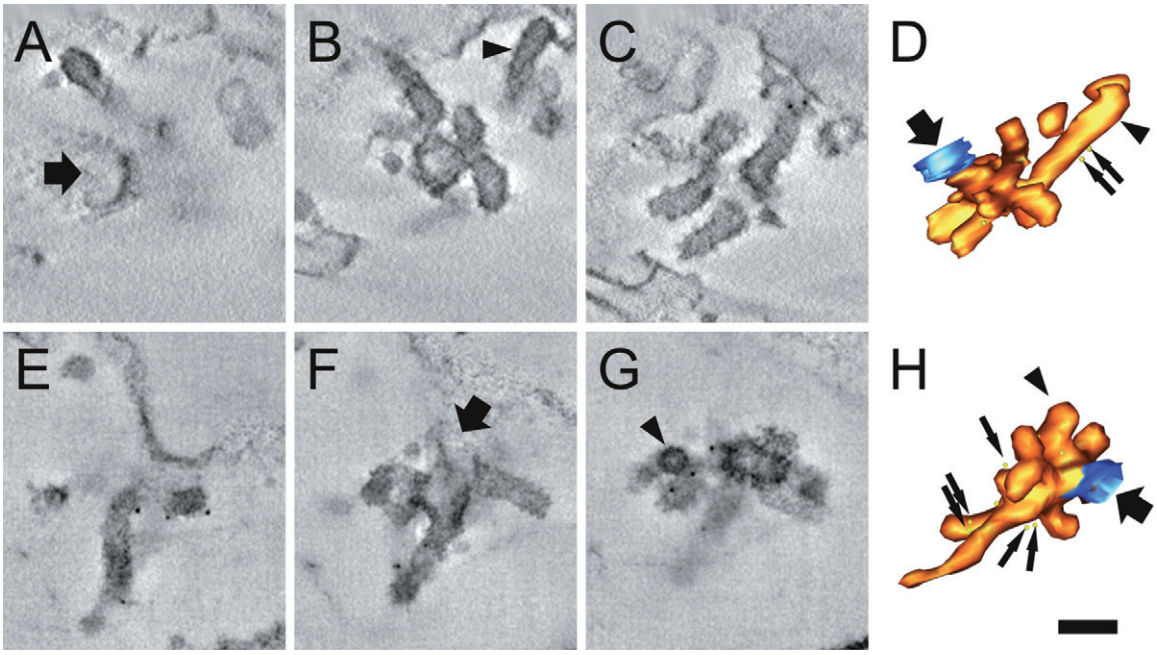

Fig. 6. Immunoelectron tomography of a CVC in a *P. cynomolgi* trophozoite iRBC.
A–H. Equinatoxin II-permeabilized *P. cynomolgi* trophozoite iRBCs were labelled with two different antibodies (A–D, mAb 4C12.G4 and E–H, rabbit anti-rPvPHIST/CVC-8195). (A–C and E–G) Selected virtual sections (20 nm) showing CVCs. (D and H) Segmentation models were created with IMOD software. The RBC membrane is rendered in blue, the CVC in orange and gold particles in yellow. The CVC opening on the surface of the iRBC is indicated by thick arrows (A, D, F, H). A long tubular extension is highlighted by an arrowhead in (B) and the same extension is shown with an arrowhead in (D). A section through one of the short tubular extensions is highlighted by an arrowhead (G) and the same extension is shown with an arrowhead in (H). The gold particles are concentrated on the tubular extensions as denoted with fine arrows (D, H). Bar: 100 nm.

EcoRI and EcoRV. The digested products that were recovered (5.1 kb and 3.6 kb) corresponded to the pUC19/*pcyΔphist81*$_{95}$ vector used to transfect the *P. cynomolgi* iRBCs (Fig. 7C). As expected, IFA and Western immunoblot experiments showed expression of the PHIST protein (Fig. 7D and E). An experiment performed in parallel, on the other hand, served as a positive control, showing the integration and expression of a red fluorescent protein (*rfp*) gene (Fig. S4; J. Jiang *et al.*, unpubl. data). These data serve to confirm for the first time that integration of a transgene is possible in *P. cynomolgi*.

Discussion

Advances in post-genomic tools and microscopic methods have greatly expanded the potential of investigations on the cellular biology of *Plasmodium* iRBCs, particularly in *P. falciparum*. The recent publication of the *P. vivax* and *P. knowlesi* genome databases (Carlton *et al.*, 2008; Pain *et al.*, 2008), and focused efforts on sequencing *P. cynomolgi* genomes (S. Tachibano *et al.*, unpubl. data), unpublished), now raise the prospects for comparable discoveries in these species. This is especially important in light of increasing data showing that *P. vivax*, in addition to causing enormous morbidity worldwide, can cause severe disease and infections that may become lethal (reviewed in Mueller *et al.*, 2009; Price *et al.*, 2009).

Plasmodium cynomolgi iRBCs are the main focus of the exploratory studies reported here, because unlike *P. vivax* they are accessible from monkey (rhesus) infections in significant numbers for experimental manipulations and in-depth investigations. Based on knowledge regarding the close phylogenetic relationship of *P. cynomolgi* and *P. vivax* and their common overarching morphological and biological features, the protein composition and functional biology of specific organelles such as the CVC are expected to be extremely similar. The current experiments are a prelude to using *P. cynomolgi* as a surrogate in expanded cell biological studies relating to CVC ultrastructure, molecular composition, and function, and, to then advance specific questions directly with *P. vivax* iRBCs attained in limited quantities from small New World monkey infections.

This study is one of only a few since 1975 to investigate the structure and molecular make-up of *Plasmodium* CVCs (Aikawa *et al.*, 1975; 1977; Barnwell, 1986; Matsumoto *et al.*, 1986; 1988; Udagama *et al.*, 1988; Atkinson and Aikawa, 1990; Barnwell *et al.*, 1990; Bracho *et al.*, 2006) and the first to present these structures in 3-D. The ET imaging results presented here corroborate previous

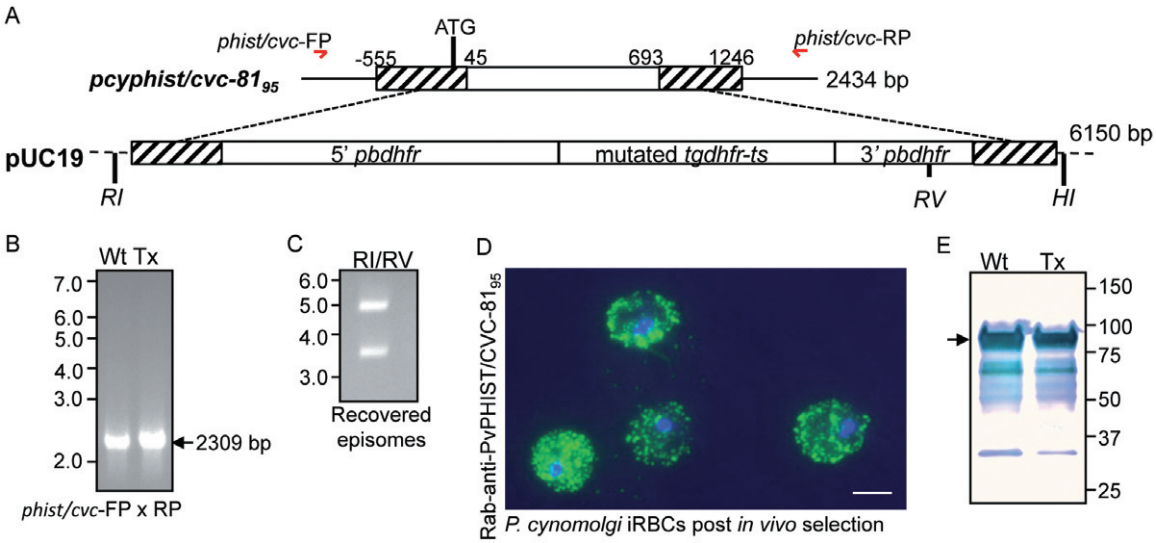

Fig. 7. *P. cynomolgi phist/cvc-81*$_{95}$ transfection experiments result in retrieval of episomes conferring resistance to pyrimethamine, but without integration in the genome. Results are shown for one of two transfection experiments.
A. Schematic of the *pcyphist/cvc-81*$_{95}$ target gene (top) and the related gene disruption vector construct with a pUC-19 backbone (bottom). Red arrows represent the location of *phist/cvc* forward (FP) and reverse (RP) oligonucleotide primers used in diagnostic PCR amplifications. The hatched boxes represent the 5′ and 3′ ends of the *pcyphist/cvc-81*$_{95}$ gene. The *pcyphist/cvc-81*$_{95}$ sequences flank the selection cassette, comprised of the *P. berghei* 5′ and 3′ UTRs and the mutated *tgdhfr-ts* gene to confer resistance to pyrimethamine. EcoRI (RI) and BamHI (HI) restriction enzyme sites were used to linearize this construct and release the selection cassette for transfection experiments.
B. Using *phist/cvc*-FP and *phist/cvc*-RP, the *pcyphist/cvc-81*$_{95}$ gene was amplified by PCR from genomic DNA purified from both wild-type (Wt) and transfected (Tx) parasites.
C. Plasmid DNA bands of 5.1 kb and 3.6 kb corresponding to the gene disruption vector were retrieved after *in vivo* selection in rhesus monkeys, purification of DNA from selected parasites, subsequent transformation of *E. coli* with this DNA, plasmid purification from the *E. coli*, and digestion with RI and EcoRV (RV) restriction enzymes.
D. IFA experiments show a normal speckled expression pattern for PHIST/CVC in Tx parasites. *P. cynomolgi* trophozoite iRBCs are shown with rabbit anti-PHIST/CVC-81$_{95}$ reactivity (green) and DAPI nuclear stain (blue). Immunofluorescence was detected using a Zeiss Imager.Z1 microscope. Scale bar: 4 μm.
E. Western immunoblot showing rabbit anti-PHIST/CVC-81$_{95}$ reactivity (95 kDa, arrow, with associated breakdown products) on both Wt and Tx trophozoite iRBCs.

TEM reports showing numerous CVCs interspersed along the surface of the *P. vivax* and *P. cynomolgi* iRBCs with their caveolae open to the surface (Aikawa *et al.*, 1975). The iRBC plasmalemma becomes highly reorganized over the course of the approximate 48 h lifespan of the growing parasites to accommodate these intricate structures. Many interesting questions remain to be answered including (i) what proteins make up these structures, (i) how are they formed, (ii) for what purpose(s) and (iv) can they become targets of intervention?

Proteomic experiments were critical to identify the *phist/cvc-81*$_{95}$ gene encoding the 95 kDa CVC antigen and designate this as a member of the PHISTc subfamily. While this protein was shown previously to be a predominant protein that is localized to the CVCs of *P. vivax* and *P. cynomolgi*, extractable primarily in SDS, and predicted to be associated with the cytoskeleton underlying the RBC membrane (Barnwell *et al.*, 1990), its gene and encoded protein characteristics had remained unknown. This discovery in fact marks the first designation of a physical location of any member of the PHIST superfamily (Sargeant *et al.*, 2006).

The tomograms show that the CVC opening (narrowing to a diameter of ~ 35 nm) has a thickened limiting membrane at the region of connection to the iRBC membrane; i.e. the electron dense caveola cup. There are five to seven tubules (~ 40 nm in diameter) emanating from each CVC opening; these tubules vary in length and can be considerably elongated (up to 400 nm). Vesicles ranging in average diameter from 25 to 45 nm are also an integral part of the CVCs, while others appear in isolation nearby. Large Maurer's cleft-like structures are also observed in the host cell cytoplasm. The cytoplasmic face of the tubules was clearly labelled with anti-PHIST/CVC-81$_{95}$ mAb and polyclonal antiserum in immuno-ET experiments, while the CVC openings, the CVC-associated vesicles and the cleft-like structures were not labelled. In previous immuno-TEM analyses, using post embedding immunolabelling procedures, several mAbs, including 2H12.G4 and 1H4.B6, stained the caveola of *P. vivax* CVCs in addition to the vesicles and tubules (Matsumoto *et al.*, 1988; Barnwell *et al.*, 1990). Future analysis of the iRBCs in different stages of development should prove to be informative with regards to the definitive static and

dynamic localization of this protein. It is certainly possible, and cannot be excluded at this time, that the protein becomes localized to and functions at the cytoplasmic interface of the CVCs, and also within the caveolae.

Different numbers and types of PHIST family members (PHISTa, PHISTb and/or PHISTc) with presumptive common ancestral lineages have been revealed in *P. falciparum*, *P. vivax*, *P. knowlesi*, *P. gallinaceum*, *P. yoelii*, *P. berghei* and *P. chabaudi* and yet neither definitive localizations nor functions have yet to be ascribed to any members. Family members can differ considerably, for example by size, structure or transcription pattern, but they all have the so-called PHIST domain in common with its characteristic multiple alpha-helices and conserved tryptophan residues (Sargeant *et al*., 2006). The presence of this domain defines family members, yet specific functions remain unknown (Sargeant *et al*., 2006). There have been 71 *phist* paralogues annotated in *P. falciparum*, 39 in *P. vivax* (18 paralogues reported in Carlton *et al*., 2008) and 27 in *P. knowlesi* (Sargeant *et al*., 2006); several PHIST proteins have also been identified in *P. cynomolgi* proteomic studies (S. Akinyi, C. Korir and M. Galinski, unpubl. data). It remains to be determined whether all genes representing members of the PHIST family are expressed in each of these species, at what stage(s), and whether the different family members have quite different or similar functions. Our BLAST searches identified which *phist* gene family member in other *Plasmodium* species is most closely related to *pvphist/cvc-81*$_{95}$ and *pcyphist/cvc-81*$_{95}$, and the comparative strong homology of this selected gene set in the 5′ and 3′ regions encoding the N- and C-terminal sequences supports their proposed relationship as orthologues. Our analyses also show that each of these genes encodes a central domain of degenerate amino acid repeated motifs, or remnants thereof (Fig. S3). The repeated motifs are evident in the *P. falciparum, P. knowlesi, P. yoelii* and *P. berghei* PHIST homologues, whereas only apparent ancestral remnants exist in the PvPHIST/CVC-81$_{95}$ and PcyPHIST/CVC-81$_{95}$ sequences, raising the possibility that the repeat motifs *per se* are not functionally important for these proteins. To the contrary, PvPHIST/CVC-81$_{95}$ and PcyPHIST/CVC-81$_{95}$ may have evolved to harness amino acid sequences that are critical for the structure and/or function of these proteins. Repeated motifs have not been previously noted as a main characteristic of PHIST family members, aside from being mentioned in one brief report (Chookajorn and Hartl, 2006). Such variable and degenerate repeated motifs are not unique to PHIST, but have become recognized as typical features of various *Plasmodium* genes and proteins (reviewed in Anders *et al*., 1993) and their intra-species sequence diversity can be high in the midst of otherwise conserved sequences (e.g. see Cowman *et al*., 1985; Galinski *et al*., 1987).

Plasmodium falciparum, P. knowlesi, P. yoelii and *P. berghei* do not produce CVCs in their host iRBC membranes, and thus the respective PHIST homologues could reasonably be expected to perform a function(s) that may be quite different from PvPHIST/CVC-81$_{95}$ and PcyPHIST/CVC-81$_{95}$. It is worth noting in this regard that PfPHIST-147 (gene ID: Pf08_0137), was found to be associated with the *P. falciparum* translocon of exported proteins (PTEX) complex (de Koning-Ward *et al*., 2009). The PTEX complex has been predicted to transport proteins from the parasite across the PV membrane to the erythrocyte cytosol. It is possible that homologous proteins, such as PHIST/CVC-81$_{95}$, with conserved PHIST domains, may have different localizations in the course of development in each species yet share common primary functions, for example, serving as protein chaperones.

Plasmodium cynomolgi as an experimental model lends itself well to exploration of the many open questions relating to the biogenesis and function of the CVCs in the biology of *P. vivax*. For example, are the caveolae and tubules of the CVCs created as a result of the invagination of the iRBC membrane at numerous points? Or, do the CVCs develop through *de novo* biogenesis from a composite of proteins, lipids and vesicles through a process of progressive or pre-formed docking at the inner surface of the infected erythrocyte membrane? The ring-stage IFA patterns representing PHIST are intriguing and distinctive compared with the later-stage parasites (Fig. 3A). The ‘soccer ball’ pattern of PHIST reactivity in these ring-stage IFAs is suggestive of a semi-organized initial placement of the CVCs at the surface of the iRBCs. If this pattern is indeed biologically relevant, perhaps the parasite requires an organized scaffold of selectively placed CVCs to brace the iRBC before progressively continuing the process of destroying and rebuilding the RBCs natural cytoskeletal architecture to accommodate an increasing number of CVCs.

While some weak and limited *in vitro* cytoadherent characteristics have been noted for *P. vivax* iRBCs (Carvalho *et al*., 2010), to date there is no evidence of a dominant cytoadhesion phenotype for *P. vivax* or *P. cynomolgi*, akin to that observed for *P. falciparum* and attributed to the adhesion of the parasite’s iRBC knobs with a variety of host endothelial receptors. *P. vivax* has no paralogues of the *var* genes of *P. falciparum*, known to encode the highly cytoadherent variant antigens (Scherf *et al*., 2008), nor the related *SICAvar* genes of *P. knowlesi* (al-Khedery *et al*., 1999; Korir and Galinski, 2006), but CVC could be a conduit for implanting members of the variable *P. vivax vir* gene family (Fernandez-Becerra *et al*., 2005) or other functional proteins into the membrane of the iRBC. That CVC participate in or regulate some necessary metabolic or physiological functions seem more likely as the primary purpose of these organelles; also making them strong

potential targets of chemical or immune intervention. By comparison, Hanssen and colleagues reported 25 nm and 80 nm diameter vesicles in *P. falciparum* iRBC (Hanssen *et al*., 2008; 2010). The 25 nm vesicles were limited by an ordinary lipid bilayer and by ET appeared to be free in the cytoplasm or associated with Maurer's clefts and the iRBC membrane. In contrast, the 80 nm vesicles had an electron-dense coat covering a 25 nm bilayer circumscribed aperture and were typically very few in number. While electron dense 'knob' protrusions are the predominant feature at the surface of *P. falciparum* iRBCs, in rare instances the 80 nm vesicles appear to have fused to the iRBC membrane to form caveolae, with a similar electron dense coat as observed for the caveolae component of the CVCs. Sparse caveolae have also been observed by TEM at the surface of *P. knowlesi* iRBCs (Aikawa *et al*., 1975). We envision that these caveolae may have a function distinct from that of the numerous CVCs found in *P. vivax* and *P. cynomolgi*.

Importantly, our replica *in vivo* transfection experiments support the hypothesis that the predominant 95 kDa CVC protein in *P. vivax* and *P. cynomolgi*, now known as PvPHIST/CVC-81$_{95}$ and PcyPHIST/CVC-81$_{95}$, is essential for parasite survival. *P. cynomolgi* parasites that had been transfected with a construct targeting the disruption of the *pcyphist/cvc-81$_{95}$* gene were selected *in vivo* in rhesus monkeys, but only parasites containing episomes with the mutated *tgdhfr* gene conferring pyrimethamine resistance survived. Our parallel experiment showing that a transgene can in fact become integrated into the *P. cynomolgi* genome is particularly important, as this is the first evidence that this is indeed possible in this species. We have concluded at this stage that the PHIST/CVC-81$_{95}$ protein is essential for the parasite. The precise roles this protein plays remains to be defined, but its abundance and prominent location suggests a critical role.

Aside from PHIST/CVC-81$_{95}$, a few other proteins have been defined in association with CVCs through either IFA or immuno-EM. These include a large (> 200 kDa) transmembrane protein (J. Barnwell and M. Galinski, unpubl. data), a 70 kDa protein (Barnwell *et al*., 1990) and an 86 kDa protein (Udagama *et al*., 1988). Caveolins and flotillin-2 have also been reported to be present within the CVCs by antibody reactivity (Bracho *et al*., 2006). In future investigations it will be important to determine the full composite of proteins associated with the CVCs, define how the CVC architecture develops during the growth of the intra-erythrocytic parasite, and identify biological and biochemical processes they serve for the parasitized cell. Given the potential in medicinal chemistry to design novel drug compounds based on structure-associated relationships, further exploration in this direction seems highly warranted to develop new drugs active against *P. vivax*.

Experimental procedures

Parasite materials

Using standard procedures, cryopreserved and reconstituted *P. cynomolgi* (Berok strain) ring iRBCs were inoculated as required into splenectomized *Macaca mulatta* (rhesus) monkeys following approved protocols from the Institutional Animal Care and Use Committee at Emory University. At an approximate 5% target parasitaemia, blood was collected and passed through glass beads and cellulose CF11 columns to remove platelets and white blood cells, respectively, and then enriched for trophozoite or schizont iRBCs by centrifugation over a 52% or 48% Percoll cushion, respectively, as described (Barnwell *et al*., 1990; Galinski *et al*., 1992).

Plasmodium cynomolgi gDNA was prepared from schizont-stage parasites using the QIAamp DNA Blood Extraction kit (Qiagen) following the manufacturer's instructions. The schizonts were obtained from fresh infected blood, as described above, or from reconstituted ring-stage iRBCs that were matured to the schizont stage in short-term culture as described (Barnwell *et al*., 1999).

Monoclonal antibodies

Monoclonal antibodies 2H8.E10, 2H12.B4, 4C12.G4 and 1H4.B6 were among a battery of mAbs raised against *P. vivax* schizont and merozoite proteins and characterized as previously described (Barnwell, 1986; Matsumoto *et al*., 1988; Barnwell *et al*., 1990). Total IgG was then purified using the Protein A MAPS affinity isolation system (Bio-Rad) following the manufacturer's protocol.

Production of recombinant protein and antisera

Pvphist/cvc-81$_{95}$ gene-specific primers PvPHIST/CVC-81$_{95}$F (5′-tat gga tcc ATG AGT CCC TGC AAC ATC) and PvPHIST/CVC-81$_{95}$R (5′-ata ctc gag TTA GAG TTT GCT GTG TTT CT) were used to amplify the full length of the gene under standard PCR conditions following the manufacturer's protocol (Calbiochem). The amplicon was cloned into the expression vector pGEX 4T-2 (GE Healthcare) using the BamHI and XhoI restriction sites. Positive clones were confirmed with an ABI 3100 DNA sequencer. The clones were then re-transformed into *E. coli* BL21 StarTM (DE3) cells (Invitrogen) for protein expression. Soluble protein was purified using Glutathione SepharoseTM 4B (GE Healthcare) slurry according to the manufacturer's protocol. Recombinant PvPHIST-81$_{95}$ (rPvPHIST/CVC-81$_{95}$) was inoculated into a New Zealand White Rabbit (Covance) for production of a polyclonal antiserum, rabbit anti-rPvPHIST/CVC-81$_{95}$.

IFA and Western immunoblots

The cross-reactivity of the mAbs raised against *P. vivax* was tested by IFA on air-dried, cold acetone-fixed thin films of RBCs infected with *P. cynomolgi* ring, trophozoite- or schizont-stage parasites. Following incubation with the primary antibodies, expression was detected using affinity-purified goat IgG anti-mouse conjugated to Alexa Fluor 488

(Invitrogen) as secondary antibodies. The mAbs were tested at 1:100, 1:200, 1:400 and 1:800 dilutions in phosphate-buffered saline (PBS; Lonza) containing 0.2% bovine serum albumin (BSA; Sigma). The rabbit anti-rPvPHIST/CVC-81_{95} IFA reactivity was tested at dilutions of 1:100, 1:200, 1:400 and 1:800, followed by anti-rabbit antibodies conjugated to Alexa Fluor 488 (Invitrogen) at a 1:200 dilution. The parasite nuclei were visualized with DAPI, contained in ProLong Gold Antifade Reagent (Invitrogen). The slides were examined with a Zeiss Imager.Z1 or Axioskope 2 microscope with filters appropriate for the fluorescent dyes, and the images merged.

For western immunoblot analyses, *P. cynomolgi* trophozoite extracts were electrophoretically separated on SDS-polyacrylamide gels and then transferred to a 0.2 μm nitrocellulose membrane (Schleicher & Schuell) and probed with the mAbs diluted 1:1000. Membranes were incubated with the corresponding alkaline phosphatase-conjugate as a secondary antibody (Promega) and immunoreactivity was detected by incubating with NBT/BCIP substrate (Promega).

Immunoprecipitation of P. cynomolgi *extracts with mAbs*

Plasmodium cynomolgi iRBC extracts were prepared as follows: ice-cold 1 × NET/1% NP-40 containing protease inhibitors (10 mM EDTA-Na2; 1 mM PMSF; 0.1 mM each of TPCK, TLCK, Leupeptin, Chymostatin, Antipain and 3,4-DCI; 10 μM EP-64 and 1 μM Pepstatin A; Sigma) was added to *P. cynomolgi*-infected erythrocyte pellet, and extracted for 30 min on ice with occasional vortexing. The samples were then transferred to pre-chilled microcentrifuge tubes and spun at 20 817 *g* for 20 min at 4°C. The resulting NP-40 extracts were transferred and stored, while the pellet was extracted in 1% SDS by occasional vortexing for 10 min at room temperature. The sample was then centrifuged at 20 817 *g* for 20 min at room temperature. The SDS extracts were combined with the NP-40 extracts for use in immunoprecipitations.

One hundred and sixty microlitres of rProtein G agarose suspension (Invitrogen) was incubated with 200 μg of each *P. vivax* mAb overnight at 4°C, rotating. Meanwhile, extracts were pre-clarified with rProtein G agarose overnight at 4°C, on a rotational shaker. The extracts were then separated from the pre-clarifying beads. Dimethyl pimelimidate (Sigma) was added to the mAb/rProtein G mix to a final concentration of 20 mM and incubated for 6 h, at 4°C, rotating. The uncoupled mAb was then removed by pulse spin, and the mixture washed with NETT (150 mM NaCl/5 mM EDTA/50 mM Tris/0.5% Triton X-100). One millilitre of the combined extract was added to the coupled mAb/rProtein G mix and incubated overnight. The beads were then washed twice with NETT, twice with NETT/0.5 M NaCl and once with NETT/0.05% SDS. The samples were resuspended in 2 × SDS-PAGE loading buffer and resolved on 4–20% gradient SDS-PAGE gels (Bio-Rad).

Mass spectrometric analysis of immunoprecipitated proteins

After resolving the extracts and membrane samples on 4–15% SDS-PAGE gradient gels, the gels were stained with colloidal Coomassie blue (Imperial Protein Stain; Thermo Scientific). Gel slices were then excised, destained, dried and processed as described (Korir and Galinski, 2006). Briefly, the gel pieces were digested with trypsin (Sigma) and the resulting peptides extracted with trifluoroacetic acid (Sigma). The samples were then desalted and concentrated using ZipTip pipette tips (Millipore). Cleaned peptides were analysed by reverse-phase LC-MS/MS (Peng and Gygi, 2001) using an LTQ-Orbitrap mass spectrometer (Thermo Finnigan). A reverse database strategy using the SEQUEST algorithm was implemented to evaluate false discovery rate; the matched peptides were filtered according to matching scores to remove all false matches from the reverse database (Peng *et al*., 2003). Only proteins that were matched by at least two peptides were accepted to further improve the confidence of identification. The peptides were then searched against the NCBI database, with searches being limited to *Plasmodium* results.

Bioinformatics for peptide and gene analyses

Protein matches acquired from LC-MS/MS were searched against *Plasmodium* (PlasmoDB; http://www.plasmodb.org) and general (National Center for Biotechnology and Information; http://www.ncbi.nlm.nih.gov/sites/entrez?db=Protein&itool=toolbar) databases to determine the homologous genes. Signal peptide cleavage sites and transmembrane domains were predicted with SignalP V3.0 (http://www.cbs.dtu.dk/services/SignalP/) and TMpred (http://www.ch.embnet.org/software/TMPRED_form.html) software respectively. Multiple alignments of PHIST protein sequences were generated using CLUSTALW2 (http://www.ebi.ac.uk/Tools/clustalw2/index.html) or the MacVector v7.2.3 software. The GOR4 program (http://npsa-pbil.ibcp.fr/cgi-bin/npsa_automat.pl?page=npsa_gor4.html; Combet *et al*., 2000) was used to predict secondary structure using the amino acid sequences of the PHIST family members.

PCR amplification and cloning of the pcyphist/cvc-81_{95} *gene*

PCR amplification of the *pcyphist/cvc-81_{95}* gene from *P. cynomolgi* gDNA was performed using a combination of *pvphist-81_{95}* and the related *pkphist-105* (Figs 2, S1 and S2) gene-specific primers and the Expand High Fidelity System (Roche) kit as per the manufacturer's protocol. PCR products were then purified using the Qiaquick purification system (Qiagen), cloned into the pCR2.1 vector (Invitrogen) and sequenced using the ABI Prism BigDye Terminator v3.0 cycle sequencing kit (Applied Biosystems). By gene walking, and the subsequent design of *pcyphist/cvc-81_{95}*-specific primers, the first 2200 nt of the *pcyphist/cvc-81_{95}* gene were sequenced and verified. To sequence the 3′ end of *pcyphist/cvc-81_{95}* up to the stop codon, degenerate reverse primers were designed based on the 3′ UTR sequences of *pvphist/cvc-81_{95}* and *pkphist-105*. The primer pair PcyPHIST/CVC.2023.F (5′-GAT GCA AGA GTA CAT TAT GC) and PcyPHIST/CVC.3′UTR.R (5′-CAA AA(A/C) GTT CTC CTA TGA CG) amplified the sequence up to the stop codon. This result was confirmed by sequencing the entire gene using *pcyphist/cvc-81_{95}*-specific primers:

PcyPHIST/CVC.1.F (5′-ATG AGT CCC TGC AAC ATC),
PcyPHIST/CVC.263.R (5′-CTC AGA GAG ATA TGC TCA AA),
PcyPHIST/CVC.566.R (5′-CAT CTC CTC CTC TTG CCA),
PcyPHIST/CVC.762R (5′-TCA GAG GGA TCG GTA TCG),
PcyPHIST/CVC.1229.R (5′-CAC CTC TTC CGT GGT ATT),
PcyPHIST/CVC.2023.F (5′-GAT GCA AGA GTA CAT TAT GC),
PcyPHIST/CVC.2160.R (5′-GAG TAT TGC ATA ATG TAC TC), and
PcyPHIST/CVC.2433.R (5′-TAC AAT TTA CTG TGT TTC TTC).

Transfection of P. cynomolgi *iRBCs*

Selection cassette. A vector with a pBlueScript backbone containing a pyrimethamine selection cassette inserted into the NdeI restriction site of the multiple cloning site was kindly provided by Alan Thomas (van der Wel *et al*., 1997). This vector includes the following gene fragments positioned head to tail: 5′ UTR sequence of *pbdhfr-ts*, mutated *tgdhfr-ts* coding sequence, and 3′ UTR sequence of *pbdhfr-ts*. Its total size is 4996 bp. Three mutations of the *tgdhfr-ts* coding sequence (Ser36Arg, Thr83Asn and Phe245Ser) required to confer resistance to pyrimethamine were confirmed by end sequencing.

Plasmodium cynomolgi phist/cvc-81$_{95}$ KO construct (pcyΔphist/cvc-81$_{95}$ vector). The following primer pairs were designed to amplify 600 bp from the 5′ region of *pyphist/cvc-81$_{95}$* (from −555 to 45) and 554 bp from the 3′ region of the *pcyphist/cvc-81$_{95}$* (from 693 to 1246): *Pcyphist/cvc-81$_{95}$* 3FP, ATTT CCCGGG AGAATGTATGATGAAGAATA; *Pcyphist/cvc-81$_{95}$* 3RP, TCCATATCAAGTCTTCCACCTCGT; *Pcyphist/cvc-81$_{95}$* 5FP, TTAAGAGAGCCA TCGATGCC; and *Pcyphist/cvc-81$_{95}$* 5RP, ATTT CCCGGG ATCATAGTAGTCATGGTTAC. The SmaI site required for subsequent reactions is underlined. All amplicons were generated using the KOD polymerase (Novagen). The 5′ and 3′ fragments were ligated using the SmaI restriction site added to the reverse primer of the 5′ region and the forward primer of the 3′ region, and amplified again with the forward primer recognizing the 5′ region and reverse primer recognizing the 3′ region. The amplicon representing the combined 5′ and 3′ fragments was inserted into the SmaI site of the pUC19 vector (New England Biolabs) to make the pUC*pcyphist5′/3′* construct. Ligation of the selection cassette into the pUC*pcyphist/cvc5′/3′* vector required the addition of a blunt restriction enzyme site to the selection cassette. Briefly, a 24 bp adaptor carrying the PmeI/NdeI/PmeI restriction site sequence was inserted into the EcoRV restriction site of pCR2.1. The selection cassette was released from the pBS vector using NdeI and then subcloned into the NdeI site of the pCR2.1 PmeI/NdeI/PmeI sequences so that the cassette could be released by digestion with PmeI. The final vector was generated by blunt end ligation of the PmeI released selection cassette into the pUC19*pcyphist/cvc5′/3′* plasmid digested with SmaI.

In vivo selection. Sequential transfection experiments were carried out, with the animal experimental protocols presented here approved by Emory University's Institutional Animal Care and Use Committee.

For each experiment, a donor rhesus macaque was inoculated with ~ 1.5×10^8 *P. cynomolgi* (Berok) ring-stage iRBCs. A blood sample was drawn when the parasitaemia reached > 4% with a majority of the iRBCs at the schizont stage. The infected blood was processed using standard procedures (Barnwell *et al*., 1999) and mature schizonts were then separated using a Percoll (Amersham) gradient of 50%, washed in RPMI and resuspended in cytomix (Kocken *et al*., 1999) at 1.5×10^9 parasites ml^{-1}. Electroporation was performed with a Bio-Rad Gene pulser II (25 μF, 200 Ohms and 2.5 kV) (van der Wel *et al*., 1997; Kocken *et al*., 1999) with 0.4 ml of an iRBC suspension mixed with 0.4 ml of linearized plasmid DNA (0.1 mg) in a 0.4 cm cuvette at room temperature. The electroporated iRBCs were resuspended in RPMI and inoculated immediately into a recipient rhesus macaque. Parasitaemias were checked daily by microscopic examination of blood smears. Once the parasitaemia was rising, doses of 1 mg kg^{-1} of pyrimethamine (Sigma) were administered, with dosing times as noted in the results section. Once the pyrimethamine-resistant parasitaemia was rising to > 3% infected blood was collected and cryopreserved using standard procedures. The animals were then treated with a standard curative regimen of chloroquine (15 mg kg^{-1} IM × 3 days) to terminate the infections.

TEM and immunolabelling

Plasmodium cynomolgi trophozoite iRBCs were fixed in incomplete RPMI-1640 containing 2% paraformaldehyde (PFA) and then permeabilized with EqtII (Anderluh *et al*., 1996) as previously described (Jackson *et al*., 2007; Hanssen *et al*., 2008). The samples were refixed in PBS containing 2% paraformaldehyde, blocked with 3% BSA in PBS and then incubated with rabbit anti-rPvPHIST-81$_{95}$ as a primary antibody in PBS/3% BSA. After washing, the cells were incubated with 6 nm gold-conjugated Protein A (Aurion) according to the manufacturer's instructions, washed again, and then fixed with 1% glutaraldehyde/0.5% PFA/0.1 M cacodylate buffer overnight. The samples were then embedded in 3% agarose and rinsed with 0.175 M cacodylate buffer. After post-fixation with 1% osmium tetroxide, the cells were stained *en bloc* with 1% uranyl acetate, and then serially dehydrated and embedded in LR White resin. The samples were sectioned to 70 nm thickness and after staining with lead citrate and uranyl acetate, observed at 120 kV on a 2010HC (Jeol, Japan) transmission electron microscope (at La Trobe University EM Facility, Melbourne).

Electron tomography

Tomography was performed as described previously (Hanssen *et al*., 2008). Sections (200–300 nm) were cut and collected on a grid and then incubated with fiducial gold particles. The sections were then contrasted with lead citrate and uranyl acetate and observed on a tilt series from −69 degrees to 69 degrees at every 1.5 degrees between captured images for the first axis and every three degrees between captured images for the second axis. Data were

acquired at an accelerating voltage of 200 kV using a Tecnai G2 TF30 transmission electron microscope (FEI, the Netherlands) at the Bio21 Institute electron microscopy facility (Melbourne). The tilt images were aligned and tomograms generated and rendered using the IMOD package (Kremer *et al*., 1996).

Nucleotide sequence accession number

The genomic sequence of *pcyphist-81*$_{95}$ was submitted to the GenBank database under Accession No. JN636815.

Acknowledgements

This research was supported by National Institutes of Health Grants AI24710 and HL0788626 and the National Center for Research Resources P51RR165 and is currently supported by the Office of Research Infrastructure Programs/OD P51OD11132. The work was also supported by funds from the Australia Research Council and the Australian National Health and Medical Research Council.

References

Aikawa, M., Miller, L.H., and Rabbege, J. (1975) Caveola–vesicle complexes in the plasmalemma of erythrocytes infected by *Plasmodium vivax* and *P. cynomolgi*. Unique structures related to Schüffner's dots. *Am J Pathol* **79:** 285–300.

Aikawa, M., Hsieh, C.L., and Miller, L.H. (1977) Ultrastructural changes of the erythrocyte membrane in ovale-type malarial parasites. *J Parasitol* **63:** 152–154.

Anderluh, G., Pungercar, J., Strukelj, B., Macek, P., and Gubensek, F. (1996) Cloning, sequencing, and expression of equinatoxin II. *Biochem Biophys Res Commun* **220:** 437–442.

Anders, R.F., McColl, D.J., and Coppel, R.L. (1993) Molecular variation in *Plasmodium falciparum*: polymorphic antigens of asexual erythrocytic stages. *Acta Trop* **53:** 239–253.

Atkinson, C.T., and Aikawa, M. (1990) Ultrastructure of malaria-infected erythrocytes. *Blood Cells* **16:** 351–368.

Aurrecoechea, C., Brestelli, J., Brunk, B.P., Dommer, J., Fischer, S., Gajria, B., *et al*. (2009) PlasmoDB: a functional genomic database for malaria parasites. *Nucleic Acids Res* **37:** D539–D543.

Barnwell, J.W. (1986) Antigens of *Plasmodium vivax* blood stage parasites identified by monoclonal antibodies. *Mem Inst Oswaldo Cruz* **81:** 59–61.

Barnwell, J.W., Ingravallo, P., Galinski, M.R., Matsumoto, Y., and Aikawa, M. (1990) *Plasmodium vivax*: malarial proteins associated with the membrane-bound caveola–vesicle complexes and cytoplasmic cleft structures of infected erythrocytes. *Exp Parasitol* **70:** 85–99.

Barnwell, J.W., Galinski, M.R., DeSimone, S.G., Perler, F., and Ingravallo, P. (1999) *Plasmodium vivax, P. cynomolgi*, and *P. knowlesi*: identification of homologue proteins associated with the surface of merozoites. *Exp Parasitol* **91:** 238–249.

Bracho, C., Dunia, I., Romano, M., Raposo, G., De La Rosa, M., Benedetti, E.L., and Perez, H.A. (2006) Caveolins and flotillin-2 are present in the blood stages of *Plasmodium vivax*. *Parasitol Res* **99:** 153–159.

Carlton, J.M., Adams, J.H., Silva, J.C., Bidwell, S.L., Lorenzi, H., Caler, E., *et al*. (2008) Comparative genomics of the neglected human malaria parasite *Plasmodium vivax*. *Nature* **455:** 757–763.

Carvalho, B.O., Lopes, S.C., Nogueira, P.A., Orlandi, P.P., Bargieri, D.Y., Blanco, Y.C., *et al*. (2010) On the cytoadhesion of *Plasmodium vivax*-infected erythrocytes. *J Infect Dis* **202:** 638–647.

Chookajorn, T., and Hartl, D.L. (2006) Position-specific polymorphism of *Plasmodium falciparum* stuttering motif in a PHISTc PFI1780w. *Exp Parasitol* **114:** 126–128.

Coatney, G.R. (1971) The simian malarias: zoonoses, anthroponoses, or both? *Am J Trop Med Hyg* **20:** 795–803.

Combet, C., Blanchet, C., Geourjon, C., and Deleage, G. (2000) NPS@: network protein sequence analysis. *Trends Biochem Sci* **25:** 147–150.

Cowman, A.F., Saint, R.B., Coppel, R.L., Brown, G.V., Anders, R.F., and Kemp, D.J. (1985) Conserved sequences flank variable tandem repeats in two S-antigen genes of *Plasmodium falciparum*. *Cell* **40:** 775–783.

Di Girolamo, F., Raggi, C., Bultrini, E., Lanfrancotti, A., Silvestrini, F., Sargiacomo, M., *et al*. (2005) Functional genomics, new tools in malaria research. *Ann Ist Super Sanita* **41:** 469–477.

Fernandez-Becerra, C., Pein, O., de Oliveira, T.R., Yamamoto, M.M., Cassola, A.C., Rocha, C., *et al*. (2005) Variant proteins of *Plasmodium vivax* are not clonally expressed in natural infections. *Mol Microbiol* **58:** 648–658.

Galinski, M., and Barnwell, J. (2012) Malaria infections in non-human primates and model systems for research. In *Nonhuman Primates in Biomedical Disease*. Abee, C., Mansfield, K., Tardif, S., and Morris, T. (eds). Oxford: Elsevier, Academic Press, pp. 299–323.

Galinski, M.R., and Barnwell, J.W. (2008) *Plasmodium vivax*: who cares? *Malar J* **7** (Suppl. 1)**:** S9.

Galinski, M.R., Arnot, D.E., Cochrane, A.H., Barnwell, J.W., Nussenzweig, R.S., and Enea, V. (1987) The circumsporozoite gene of the *Plasmodium cynomolgi* complex. *Cell* **48:** 311–319.

Galinski, M.R., Medina, C.C., Ingravallo, P., and Barnwell, J.W. (1992) A reticulocyte-binding protein complex of *Plasmodium vivax* merozoites. *Cell* **69:** 1213–1226.

Galinski, M.R., Dluzewski, A.R., and Barnwell, J.W. (2005) Malaria merozoites and invasion of erythrocytes. In *Molecular Approaches to Malaria*. Sherman, I.W. (ed.). New York: ASM Press, pp. 113–168.

Gardner, M.J., Hall, N., Fung, E., White, O., Berriman, M., Hyman, R.W., *et al*. (2002) Genome sequence of the human malaria parasite *Plasmodium falciparum*. *Nature* **419:** 498–511.

Haase, S., and de Koning-Ward, T.F. (2010) New insights into protein export in malaria parasites. *Cell Microbiol* **12:** 580–587.

Hanssen, E., Sougrat, R., Frankland, S., Deed, S., Klonis, N., Lippincott-Schwartz, J., and Tilley, L. (2008) Electron tomography of the Maurer's cleft organelles of *Plasmodium falciparum*-infected erythrocytes reveals novel structural features. *Mol Microbiol* **67:** 703–718.

Hanssen, E., Goldie, K.N., and Tilley, L. (2010) Ultrastructure

of the asexual blood stages of *Plasmodium falciparum*. *Methods Cell Biol* **96:** 93–116.
Hanssen, E., Knoechel, C., Klonis, N., Abu-Bakar, N., Deed, S., LeGros, M., *et al.* (2011) Cryo transmission X-ray imaging of the malaria parasite, *P. falciparum*. *J Struct Biol* **173:** 161–168.
Hiller, N.L., Bhattacharjee, S., van Ooij, C., Liolios, K., Harrison, T., Lopez-Estrano, C., and Haldar, K. (2004) A host-targeting signal in virulence proteins reveals a secretome in malarial infection. *Science* **306:** 1934–1937.
Jackson, K.E., Spielmann, T., Hanssen, E., Adisa, A., Separovic, F., Dixon, M.W., *et al.* (2007) Selective permeabilization of the host cell membrane of *Plasmodium falciparum*-infected red blood cells with streptolysin O and equinatoxin II. *Biochem J* **403:** 167–175.
al-Khedery, B., Barnwell, J.W., and Galinski, M.R. (1999) Antigenic variation in malaria: a 3′ genomic alteration associated with the expression of a *P. knowlesi* variant antigen. *Mol Cell* **3:** 131–141.
Kocken, C.H., van der Wel, A., and Thomas, A.W. (1999) *Plasmodium cynomolgi*: transfection of blood-stage parasites using heterologous DNA constructs. *Exp Parasitol* **93:** 58–60.
de Koning-Ward, T.F., Gilson, P.R., Boddey, J.A., Rug, M., Smith, B.J., Papenfuss, A.T., *et al.* (2009) A newly discovered protein export machine in malaria parasites. *Nature* **459:** 945–949.
Korir, C.C., and Galinski, M.R. (2006) Proteomic studies of *Plasmodium knowlesi* SICA variant antigens demonstrate their relationship with *P. falciparum* EMP1. *Infect Genet Evol* **6:** 75–79.
Kremer, J.R., Mastronarde, D.N., and McIntosh, J.R. (1996) Computer visualization of three-dimensional image data using IMOD. *J Struct Biol* **116:** 71–76.
Maier, A.G., Cooke, B.M., Cowman, A.F., and Tilley, L. (2009) Malaria parasite proteins that remodel the host erythrocyte. *Nat Rev Microbiol* **7:** 341–354.
Marti, M., Good, R.T., Rug, M., Knuepfer, E., and Cowman, A.F. (2004) Targeting malaria virulence and remodeling proteins to the host erythrocyte. *Science* **306:** 1930–1933.
Matsumoto, Y., Matsuda, S., and Yoshida, Y. (1986) Ultrastructure of human erythrocytes infected with *Plasmodium ovale*. *Am J Trop Med Hyg* **35:** 697–703.
Matsumoto, Y., Aikawa, M., and Barnwell, J.W. (1988) Immunoelectron microscopic localization of vivax malaria antigens to the clefts and caveola–vesicle complexes of infected erythrocytes. *Am J Trop Med Hyg* **39:** 317–322.
Mueller, I., Galinski, M.R., Baird, J.K., Carlton, J.M., Kochar, D.K., Alonso, P.L., and del Portillo, H.A. (2009) Key gaps in the knowledge of *Plasmodium vivax*, a neglected human malaria parasite. *Lancet Infect Dis* **9:** 555–566.
Pain, A., Bohme, U., Berry, A.E., Mungall, K., Finn, R.D., Jackson, A.P., *et al.* (2008) The genome of the simian and human malaria parasite *Plasmodium knowlesi*. *Nature* **455:** 799–803.
Peng, J., and Gygi, S.P. (2001) Proteomics: the move to mixtures. *J Mass Spectrom* **36:** 1083–1091.
Peng, J., Elias, J.E., Thoreen, C.C., Licklider, L.J., and Gygi, S.P. (2003) Evaluation of multidimensional chromatography coupled with tandem mass spectrometry (LC/LC-MS/MS) for large-scale protein analysis: the yeast proteome. *J Proteome Res* **2:** 43–50.
Pfahler, J.M., Galinski, M.R., Barnwell, J.W., and Lanzer, M. (2006) Transient transfection of *Plasmodium vivax* blood stage parasites. *Mol Biochem Parasitol* **149:** 99–101.
Price, R.N., Douglas, N.M., and Anstey, N.M. (2009) New developments in *Plasmodium vivax* malaria: severe disease and the rise of chloroquine resistance. *Curr Opin Infect Dis* **22:** 430–435.
Rowe, J.A., Opi, D.H., and Williams, T.N. (2009) Blood groups and malaria: fresh insights into pathogenesis and identification of targets for intervention. *Curr Opin Hematol* **16:** 480–487.
Sargeant, T.J., Marti, M., Caler, E., Carlton, J.M., Simpson, K., Speed, T.P., and Cowman, A.F. (2006) Lineage-specific expansion of proteins exported to erythrocytes in malaria parasites. *Genome Biol* **7:** R12.
Scherf, A., Lopez-Rubio, J.J., and Riviere, L. (2008) Antigenic variation in *Plasmodium falciparum*. *Annu Rev Microbiol* **62:** 445–470.
Schüffner, W. (1899) Beitrag zur kenntniss der malaria. *Dtsch Arch Klin Med* **64:** 428–449.
Spielmann, T., and Gilberger, T.W. (2010) Protein export in malaria parasites: do multiple export motifs add up to multiple export pathways? *Trends Parasitol* **26:** 6–10.
Tilley, L., Sougrat, R., Lithgow, T., and Hanssen, E. (2008) The twists and turns of Maurer's cleft trafficking in *P. falciparum*-infected erythrocytes. *Traffic* **9:** 187–197.
Tilley, L., Dixon, M.W., and Kirk, K. (2011) The *Plasmodium falciparum*-infected red blood cell. *Int J Biochem Cell Biol* **43:** 839–842.
Trager, W., and Jensen, J.B. (1976) Human malaria parasites in continuous culture. *Science* **193:** 673–675.
Udagama, P.V., Atkinson, C.T., Peiris, J.S., David, P.H., Mendis, K.N., and Aikawa, M. (1988) Immunoelectron microscopy of Schüffner's dots in *Plasmodium vivax*-infected human erythrocytes. *Am J Pathol* **131:** 48–52.
Waters, A.P., Higgins, D.G., and McCutchan, T.F. (1993) The phylogeny of malaria: a useful study. *Parasitol Today* **9:** 246–250.
van der Wel, A.M., Tomas, A.M., Kocken, C.H., Malhotra, P., Janse, C.J., Waters, A.P., and Thomas, A.W. (1997) Transfection of the primate malaria parasite *Plasmodium knowlesi* using entirely heterologous constructs. *J Exp Med* **185:** 1499–1503.
WHO (2011) *World Malaria Report*. Geneva: World Health Organization, p. ix.

Supporting information

Additional supporting information may be found in the online version of this article.

Please note: Wiley-Blackwell are not responsible for the content or functionality of any supporting materials supplied by the authors. Any queries (other than missing material) should be directed to the corresponding author for the article.